Journal of Organometallic Chemistry 887 (2019) 24–31

Contents lists available at ScienceDirect

Journal of Organometallic Chemistry

journal homepage: www.elsevier.com/locate/jorganchem

Accessing copper-tin-sulfide nanostructures from diorganotin(IV) and copper(I) 2-pyrazinyl thiolates

Adish Tyagi [a, b], Goutam Kumar Kole [c], Alpa Y. Shah [a], Amey Wadawale [a], A.P. Srivastava [d], Mukesh Kumar [e], G. Kedarnath [a, b, *], Vimal K. Jain [f, **]

[a] Chemistry Division, Bhabha Atomic Research Centre, Mumbai, 400 085, India
[b] Homi Bhabha National Institute, Anushaktinagar, Mumbai, 400 094, India
[c] Department of Chemistry and Research Institute, SRM Institute of Science and Technology, Kattankulathur, Tamil Nadu, 603203, India
[d] Materials Science Division, Bhabha Atomic Research Centre, Mumbai, 400 085, India
[e] Radiation Biology and Health Sciences Division, Bhabha Atomic Research Centre, Trombay, Mumbai, 400085, India
[f] UM-DAE Centre for Excellence in Basic Sciences, University of Mumbai, Kalina Campus, Mumbai, 400 098, India

ARTICLE INFO

Article history:
Received 30 August 2018
Received in revised form
1 February 2019
Accepted 27 February 2019
Available online 1 March 2019

Keywords:
Diorganotin(IV)thiolate
Copper(I)thiolate
Molecular precursors
Metal sulfide
CTS nanostructure

ABSTRACT

Synthesis of air stable di-*tert*-butyltin(IV) and copper(I) complexes of 2-pyrazinyl thiolate (2-pyzSH), [^{t}Bu$_2$Sn(Spyz)$_2$] (**1**) and [Cu(Spyz)(PPh$_3$)$_2$] (**2**), as molecular precursors for metal sulfide nanomaterials is described. These complexes were isolated by the reactions of [^{t}Bu$_2$SnCl$_2$] and [CuCl(PPh$_3$)$_3$] with sodium 2-pyrazinyl thiolate at room temperature. The molecular structures of these complexes have been established by single crystal X-ray diffraction analyses and hetero nuclear NMR. The thermal analyses of **1** and **2** revealed closely related decomposition temperatures with the formation of the corresponding metal sulfide. Utility of these complexes as molecular precursors for the preparation of binary (SnS and Cu$_{1.8}$S) and ternary Cu$_2$SnS$_3$ (CTS) metal sulfide nanostructures has been assessed. The phase purity, morphology and composition of nanostructures were investigated by PXRD, Raman, SEM, TEM and EDS analysis. The band gap of nanostructures as deduced from diffuse reflectance spectroscopy (DRS) are 1.4, 1.8 and 2.0 eV for CTS, SnS and Cu$_{1.8}$S, respectively which are blue shifted relative to their respective bulk counterpart. It has been demonstrated that role of solvent is highly crucial for the phase purity of CTS nanostructures. The Photo-electrochemical studies revealed that CTS nanostructures pose as better photo responsive material as compared to Cu$_{1.8}$S.

1. Introduction

Ever increasing environmental and energy concerns have led to an insatiable quest for non-toxic and earth abundant materials for solar cell applications [1]. In this context various copper based ternary CuInSe$_2$ and quaternary Cu(In,Ga)Se$_2$, Cu$_2$ZnSnS$_4$ (CZTS) and Cu$_2$ZnSnSe$_4$ (CZTSe) chalcogenides have been intensively explored as absorbing material for photovoltaic devices [2,3]. However, scarcity of gallium and indium and structural complexities associated with quaternary CZTS, may limit their use for practical applications [4,5]. Recently, ternary materials, such as Cu$_2$SnS$_3$ (CTS), in their nano regime have attracted considerable attention due to solution processability and low cost. CTS is also projected as substitute for the technologically well-established solar cell materials which are based either on scarce (In,Te) or toxic (Cd, Pb) elements [4,6].

Dicopper tin trisulfide (Cu$_2$SnS$_3$, CTS), a p-type semiconductor, stands out for its high absorption coefficient (>10^4 cm^{-1}), tuneable band gap varying between 0.9 and 1.7 eV which covers the optimal solar spectrum [7,8], reasonably good electrical properties and composed of earth abundant elements making it cost effective [9].

CTS nanostructures have been synthesized earlier via chemical route such as hydrothermal [10], microwave [11], solvothermal [12,13] and hot injection methods [14–16]. These synthesis routes mostly employ suitable sulfur source such as sulfur powder [15], thiourea, thioacetamide [10], 1-dodecanethiol [12], 1-octadecene/oleic acid – sulfur precursor [17] and metal halides or acetate. However, synthesis of ternary and quaternary materials is generally

* Corresponding author. Chemistry Division, Bhabha Atomic Research Centre, Mumbai, 400 085, India.
** Corresponding author.
E-mail addresses: kedar@barc.gov.in (G. Kedarnath), jainvk@cbs.ac.in (V.K. Jain).

https://doi.org/10.1016/j.jorganchem.2019.02.026
0022-328X/

encountered with problem of presence of binary impurities [5]. Molecular precursor route has remarkable potential to be used in the synthesis of these compounds due to advantages associated with it in terms of lower defect concentration, phase purity, narrow size distribution and better control over the composition of complex material. Therefore, our previous efforts include precursor design for various metal chalcogenide materials.

We have employed molecular precursor approach for the synthesis of metal chalcogenide nano-materials and for deposition of thin films [18]. Previously we have successfully demonstrated the utility of $[R_2Sn(2\text{-}SC_5H_4N)_2]$, $[R_2SnCl\{SC_4H(Me\text{-}4,6)_2N_2\}]$ [19], $[Ag_3(\mu\text{-}Se\text{-}4\text{-}py)_3(PPh_3)_4]_2$, $[Ag_2(\mu\text{-}S\text{-}4\text{-}py)_2(PPh_3)_4]$, $[Ag(S\text{-}4\text{-}py)]_n$ [20], $[Cu\{SeC_5H_3(Me\text{-}3)N\}]_4$ [21], $[Cu\{SeC_4H(Me\text{-}4,6)_2N_2\}]_6$ [22], $[R_2Sn\{SeC_5H_3(Me\text{-}3)N\}_2]$ [23], $[R_2Sn\{SeC_4H(Me\text{-}4,6)_2N_2\}_2]$ [24] and $[In\{SeC_5H_3(Me\text{-}3)N\}_3]$ [25], precursors for the synthesis of metal chalcogenide nanocrystals and deposition of thin films. Apart from the synthesis of binary materials, these precursors have also been used for the preparation of ternary metal chalcogenides (e.g., $CuInSe_2$, Cu_2SnSe_3) [25,26].

To the best of our knowledge, there is hardly any report for the synthesis of CTS nanostructures through molecular precursor route. Thus, it was considered worthwhile to extend this strategy for the synthesis of technologically important ternary sulfide (CTS). Accordingly, air stable organotin and copper precursor derived from 2-pyrazinyl thiolate have been synthesized and conveniently used for the preparation of both binary (SnS and $Cu_{1.8}S$) and ternary (CTS) metal sulfide nanostructures. It has also been demonstrated that choice of solvent is indispensable for obtaining phase pure ternary chalcogenide material. The results of this work are described herein.

2. Experimental

Di-*tert*-butyltindichloride, anhydrous CuCl, triphenylphosphine, oleylamine (OLA), octadecene (ODE), oleic acid (OA) and analytical grade solvents were procured from commercial sources and were used without further purification. 2-Mercapto pyrazine (2-pyzSH) [m.p.: 216 °C (decomp.); Anal Calcd. for $C_4H_4N_2S$: C, 42.83; H, 3.59; N, 24.97; Found: C, 42.97; H, 3.51; N, 24.83; ^{1}H NMR (300 MHz, $CDCl_3$)δ_H: 8.88 (d, 1H), 8.63 (dd, 1H), 8.42 (d, 1H)] was prepared according to literature method [27]. Various instrumental techniques and procedures used during this investigation are given in the supplementary information.

2.1. Synthesis of complexes

2.1.1. [^{t}Bu$_2$Sn(Spyz)$_2$] (**1**)

To a methanolic solution (20 ml) of sodium pyrazinyl-2-thiolate, obtained from 2-mercaptopyrazine (200 mg, 1.78 mmol) in methanol and sodium methoxide (0.2 M, 9 ml), solid ^{t}Bu$_2$SnCl$_2$ (270 mg, 0.89 m mol) was added with stirring which continued for 2 h at room temperature until a turbid solution appeared. The contents were filtered through a G-3 filtering unit and the filtrate on slow evaporation afforded pale yellow crystals of the title complex (yield: 298 mg, 74%), mp 120 °C. Anal. Calcd for $C_{16}H_{24}N_4S_2Sn$: C, 42.21; H, 5.31; N, 12.3%. Found: C, 42.08; H, 5.22; N, 12.11%. ^{1}H NMR (300 MHz, $CDCl_3$) δ_H: 1.35 (s, ^{t}Bu$_2$Sn, 18H, $^3J(^{119}Sn\text{-}^1H) = 110$ Hz; $^3J(^{117}Sn\text{-}^1H) = 105$ Hz); 8.12 (dd, CH-5, 2H, 3.1 Hz); 8.2 (d, CH-5, 2H, 2.7 Hz); 8.58 (d, CH-3, 2H, $^4J = 1.5$ Hz); ^{119}Sn{^{1}H} NMR (111.92 MHz, $CDCl_3$) δ_{Sn}: -18.4 ppm.

2.1.2. [Cu(Spyz)(PPh$_3$)$_2$] (**2**)

To a methanolic solution of 2-pyzSNa (obtained by adding NaOH (aq, 80 mg, 2 mmol) to 2-pyzSH (225 mg, 2 mmol) in 15 ml methanol) $[CuCl(PPh_3)_3]$ (1.77 g, 2 mmol) dispersed in 15 ml acetonitrile was added with stirring which was continued for 2 h at room temperature. Block-shaped orange single crystals were obtained after a few days upon slowly evaporating orange solution. Yield: 1.07 g (76.5%), mp 102 °C. Anal. Calcd for $C_{40}H_{33}CuN_2P_2S$: C, 68.70; H, 4.75; N, 4.00; S, 4.58%. Found: C, 69.06; H, 4.98; N, 3.93; S, 3.6%. ^{1}H NMR (300 MHz, $CDCl_3$): $\delta_H = 8.46$ (s, 1H), 7.73 (d, 1H, 2.4 Hz), 7.43 (d, 1H, 2.4 Hz), 7.35–7.21 (m, 30H, PPh_3). ^{31}P{^{1}H} NMR (121.49 MHz, $CDCl_3$): $\delta_P = -2.9$ ppm (Cu-PPh_3).

2.2. Preparation of copper tin sulfide nanostructures

The CTS nanostructures were synthesized by heat up method using [^{t}Bu$_2$Sn(Spyz)$_2$] (**1**) and [Cu(Spyz)(PPh$_3$)$_2$] (**2**) as molecular precursors. In a typical experiment, [^{t}Bu$_2$Sn(Spyz)$_2$] (**1**) (32.5 mg, 0.07 mmol) and [Cu(Spyz)(PPh$_3$)$_2$] (**2**) (100 mg, 0.14 mmol) were dispersed in 8 ml of the high boiling solvent (OA and OLA either individually or in combination) in a three-necked flask and degassed under nitrogen flow at room temperature. The reaction temperature was raised to 300 °C and kept at that temperature for 20 min. The dark turbid solution was rapidly cooled to 70 °C where excess methanol was injected into the flask. The resulting nanocrystals were separated by centrifugation and purified by washing several times with 2:1 mixture of methanol and toluene solution and dried.

A similar experiment was carried out in OLA at lower temperature 275 °C. The reaction mixture containing complexes **1** and **2** were heated to 275 °C and kept at that temperature for 20 min. The nanostructures were isolated as mentioned above.

In addition to the preparation of CTS nanostructures, the thermolysis of molecular precursors **1** and **2** were carried out separately in OLA at 300 °C for 20 min to obtain tin sulfide and copper sulphide nanostructures respectively which were used as references while assessing the phase purity of CTS nanostructures.

3. Results and discussion

3.1. Synthesis and spectroscopy

The ^{1}H, ^{31}P{^{1}H}, ^{1109}Sn{^{1}H} NMR spectra were recorded in $CDCl_3$ [Figs. S1–4] (ESI†). The ^{1}H NMR spectra of the complexes exhibited expected resonances and peak multiplicities. The ^{31}P spectrum of complex (**2**) displayed a resonance at $\delta \sim -2.9$ due to coordinated PPh_3 ligands. For complex (**1**), the $^3J(^{119}Sn\text{-}^1H)$ is ~110 Hz which is in close agreement with the values reported for di-*t*-butyl tin compounds [28,29]. The ^{119}Sn{^{1}H} NMR spectrum showed a single resonance ruling out any possibility of the existence of more than one species in solution. ^{119}Sn signals for four and six coordinate compounds are observed in the range of $\delta = +200$ to -60 and -200 to -400 ppm, respectively [30,31]. The peak at $\delta = -18$ ppm is well within the former range indicating a four coordination around tin devoid of any weak interaction between Sn and N of pyrazine ring in solution phase. This may be possibly due to the inductive and steric effects of the ^{t}Bu group in organotin complexes which reduces the acceptor properties of tin [23,24].

The molecular structures of [^{t}Bu$_2$Sn(Spyz)$_2$] (**1**) and [Cu(S-pyz)(PPh$_3$)$_2$] (**2**), established by single crystal X-ray diffraction analyses are shown in Figs. 1 and 2. Selected inter-atomic parameters are given in Table 1. Compound **1** crystallizes in orthorhombic space group *Pbca*. The coordination around tin is defined by two ^{t}Bu groups and two thiolate sulfur atoms. The Sn–C and Sn–S bond distances (Table 1) are well in agreement with those reported for diorganotin bis thiolates derived from N-heterocyclic thiolates ligands [19,32–34]. The distances between tin and ortho-N of pyrazinyl rings (Sn1···N1 = 2.88 Å & Sn1···N3 = 2.90 Å) are longer than the sum of their covalent radii (2.15 Å) but are shorter than the sum

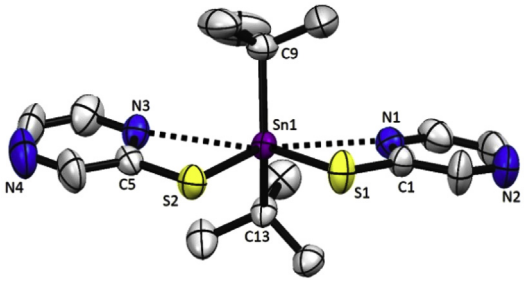

Fig. 1. Molecular structure of [^{t}Bu$_2$Sn(Spyz)$_2$] (**1**) with partial atomic numbering scheme. Hydrogen atoms are omitted for clarity. Ellipsoids are drawn with 50% probability. The shorter distance between Sn and N atoms, Sn1-N1and Sn1-N3 are 2.88 and 2.90 Å respectively, suggest weak interaction exist between them.

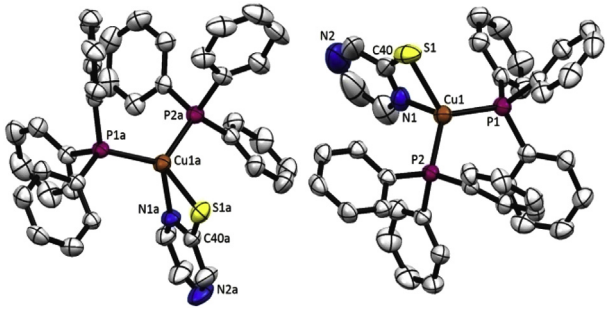

Fig. 2. Molecular structure of [Cu(Spyz)(PPh$_3$)$_2$] (**2**) with partial atomic numbering scheme. There are two molecules in asymmetric unit. Hydrogen atoms are omitted for clarity. Ellipsoids are drawn with 50% probability.

of van der Waal's radii (3.72 Å) indicating a weak interaction between them, which appears to have been diminished in solution. Such interaction between Sn and N is distinctly different from analogus diorganotin bis(2-pyridylthiolates), [R$_2$Sn(Spy)$_2$] (R = Me, Et, Ph) [19,32,33] and [^{n}Bu$_2$Sn{SC$_5$H$_3$(5-NO$_2$)N}$_2$] [34] which exhibit relatively stronger Sn–N bonding interactions as evident from much shorter Sn···N distances (2.52–2.63 Å). This can be attributed to steric demand of ^{t}Bu groups attached to tin which forces two pyrazinyl ring to occupy space at a larger distance from the tin atoms.

Compound **2** crystallizes in triclinic space group $P\bar{1}$. The copper atom acquires a distorted tetrahedral configuration defined by two P atoms of PPh$_3$ ligand and N and S atoms from chelating pyrazine-2-thiolate group. There are two molecules of [Cu(Spyz)(PPh$_3$)$_2$] present in the crystallographic asymmetric unit which differs slightly in their inter-atomic parameters. One of these molecule forms dimeric units with similar neighbouring molecule through weak attractive intermolecular N···H–C(N) interactions between the pyrazinyl rings whereas the other one is devoid of any such intermolecular contacts (Fig. S5) (ESI†). The Cu–S, Cu–N, and Cu–P bond distances (Table 1) are normal and are in conformity with those reported in literature [35,36].

3.2. Thermogravimetric analyses

Thermogravimetric analyses (TGA) were carried out to evaluate the thermal decomposition behaviour of the complexes under flowing argon atmosphere (Fig. 3). TG curve for [^{t}Bu$_2$Sn(Spyz)$_2$] (**1**) shows a single step decomposition at around 275 °C with the weight of residue (33.7%) corresponding to SnS (32.9%). Similarly the TG curve of [Cu(Spyz)(PPh$_3$)$_2$] (**2**) showed a single step decomposition of the complex taking place at 335 °C with weight loss found (86.6%) which is in agreement with the calculated weight loss (86.4%) expected for the formation of CuS.

3.3. Preparation and characterization of the nanostructures

Several synthetic methodologies have been developed for the preparation of CTS nanostructures. However, compared to binary chalcogenides, it is a challenging task to control stoichiometry and phase purity of ternary nanostructures due to the different reactivities of the metal precursors. To prepare ternary nanostructures, it is essential to select suitable combination of precursor material having similar kind of reactivities and comparable decomposition temperatures. The complexes **1** and **2** shows closely related decomposition temperature and give respective metal sulfide upon decomposition as evident from thermogravimetric analysis. Thus, these complexes were chosen to assess their utility as molecular precursors for the preparation of ternary copper tin sulphide (CTS) nanostructures. The crystal structure, morphology, homogeneity and band gap of the resulting products were characterized by powder X-ray diffraction (PXRD), Raman spectroscopy, energy dispersive X-ray analysis (EDX), SEM, TEM, selective area electron diffraction (SAED) techniques, solid state diffuse reflectance spectroscopy.

The CTS nanostructures were prepared by heat up method in three distinct high boiling solvent systems (OA, OA-OLA mixture (1:1, v/v) and OLA). Different solvent systems were chosen to

Table 1
Selected bond lengths (Å) and angles (°) of [^{t}Bu$_2$Sn(Spyz)$_2$] (**1**) and [Cu(Spyz)(PPh$_3$)$_2$] (**2**).

[^{t}Bu$_2$Sn(Spyz)$_2$] (**1**)		[Cu(Spyz)(PPh$_3$)$_2$] (**2**)			
		Molecule I		Molecule II	
C9–Sn1	2.203(6)	Cu1a–S1a	2.4395(11)	Cu1–S1	2.4358(13)
C13–Sn1	2.207(5)	Cu1a–N1a	2.141(3)	Cu1–N1	2.131(4)
S1–Sn1	2.5075(15)	Cu1a–P1a	2.2422(10)	Cu1–P1	2.2504(11)
S2–Sn1	2.4939(16)	Cu1a–P2a	2.2591(11)	Cu1–P2	2.2407(11)
S1–C1	1.745(6)	S1a–C40a	1.728(4)	S1–C40	1.701(7)
S2–C5	1.724(6)				
Sn1–N1	2.886				
Sn1–N3	2.902				
C9–Sn1–C13	128.6(2)	S1a–Cu1a–N1a	69.12(10)	S1–Cu1–N1	68.51(13)
C9–Sn1–S1	106.49(17)	S1a–Cu1a–P1a	120.99(4)	S1–Cu1–P1	117.12(5)
C9–Sn1–S2	110.42(16)	S1a–Cu1a–P2a	116.50(4)	S1–Cu1–P2	117.86(4)
C13–Sn1–S1	110.77(15)	N1a–Cu1a–P1a	115.77(10)	N1–Cu1–P1	109.35(11)
C13–Sn1–S2	107.29(17)	N1a–Cu1a–P2a	105.24(9)	N1–Cu1–P2	114.70(11)
S1–Sn1–S2	84.34(5)	P1a–Cu1a–P2a	117.60(4)	P1–Cu1–P2	118.42(4)
N3–Sn1–N1	160.47				

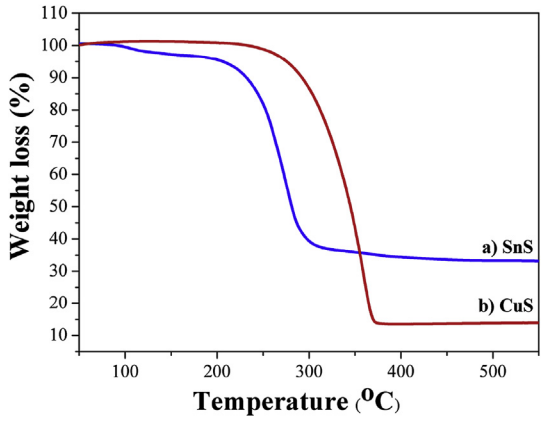

Fig. 3. Thermogravimetric analysis data for complexes a) [^{t}Bu$_2$Sn(Spyz)$_2$] (**1**) and b) [Cu(Spyz)(PPh$_3$)$_2$] (**2**) respectively.

evaluate the effect of capping agents with different binding ability on the phase purity and morphology of nanostructures. Active −COOH group of OA and oleate ions, obtained from the mixture of OA-OLA has high electron donating and strong binding ability thus making them a strong capping agent whereas OLA is relatively weaker capping agent but provide strong reducing atmosphere at an elevated temperature. In a typical heat up experiment, the complexes **1** and **2** were dispersed in different high boiling solvent systems at room temperature and slowly heated whereupon a clear yellow solution formed at ~120 °C, which turned orange to red (~190 °C) finally became black (~230 °C). This colour change is indicative of the formation and growth of the metal chalcogenide nanostructures. The heating of reaction mixture continued to desired growth temperature, i.e. 300 °C for 20 min followed by quenching and purification of the nanostructures.

The samples prepared in different reaction solvents are initially analysed by the PXRD in order to assess phase purity, crystallinity and crystal structure of CTS nanostructures. The XRD patterns of CTS nanostructures synthesized at same growth temperature (300 °C) and duration (20 min) using different solvent systems showed different profile suggesting the formation of different

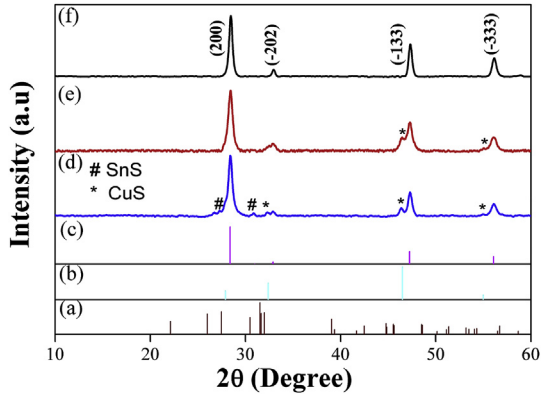

Fig. 4. a), b), c) are the simulated XRD patterns of orthorhombic SnS (JCPDS no. 75-0925), cubic Cu$_{1.8}$S (JCPDS no. 04-004-7716), monoclinic CTS (JCPDS no. 04-010-5719) respectively. XRD profiles of CTS nanostructures obtained by thermolysis of complex **1** and **2** at 300 °C for 20 min by heat up method in d) OA-OLA, e) OA and f) OLA as solvent/capping agent respectively. (# indicates impurity peaks of orthorhombic SnS while * indicates the impurity peak of cubic Cu$_{1.8}$S).

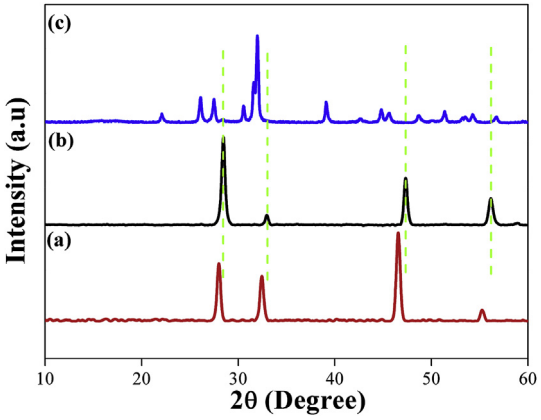

Fig. 5. PXRD patterns of a) cubic Cu$_{1.8}$S, b) monoclinic CTS and c) orthorhombic SnS obtained by thermolysis of complex (**1**) and (**2**) either individually or in combination at 300 °C for 20 min by heat up method in OLA as solvent/capping agent.

Table 2
Reaction condition, structural, morphological, compositional and optical parameters of nanostructures.

Nanostructure	Reaction solvent	Crystallite size (nm)	Morphology	EDS analysis	Optical band gap (eV)
Phase pure CTS	OLA	22	Spherical particles	2.1:1.0:3.0 (Cu:Sn:S)	1.4
Phase pure SnS	OLA	27	Rectangular sheets	1:1 (Sn:S)	1.8
Phase pure Cu$_{1.8}$S	OLA	13	Hexagonal discs	1.6:1 (Cu:S)	2.0
CTS with SnS and CuS impurity	OA	~15	Agglomeration of particles	3.4:1.0:3.8 (Cu:Sn:S)	
CTS with CuS impurity	OA-OLA	~15	Agglomeration of particles along with rectangular sheets	3.6:1.0:4.4 (Cu:Sn:S)	

Table 3
Lattice parameter of nanostructures (CTS, SnS and Cu$_{1.8}$S) synthesized in OLA at 300 °C.

Precursor	Nanostructures	Lattice parameter					
		a (Å)	b (Å)	c (Å)	α (°)	β (°)	γ (°)
[^{t}Bu$_2$Sn(Spyz)$_2$] (**1**) + [Cu(Spyz)(PPh$_3$)$_2$] (**2**)	Monoclinic CTS	6.638(8)	11.513(6)	6.645(2)	90	109.29(8)	90
[^{t}Bu$_2$Sn(Spyz)$_2$] (**1**)	Orthorhombic SnS	3.963(4)	4.350(8)	11.13(5)	90	90	90
[Cu(Spyz)(PPh$_3$)$_2$] (**2**)	Cubic Cu$_{1.8}$S	5.561(1)			90	90	90

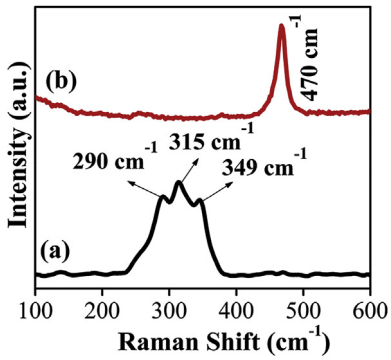

Fig. 6. Raman spectra of a) monoclinic CTS and b) cubic $Cu_{1.8}S$ obtained by thermolysis of precursors in OLA at 300 °C.

products (Fig. 4d–f). Clearly the nature of the solvent affected the formation of desired product.

Thermolysis of complexes either in OA or in a mixture of OA-OLA revealed the formation of monoclinic phase of CTS as a major product slightly contaminated by cubic phase of $Cu_{1.8}S$. Low intensity peaks in PXRD at $2\theta = 32.43, 46.40$ and $54.98°$ are attributed to (200), (220) and (311) crystal planes confirming the presence of $Cu_{1.8}S$ (JCPDS 04-006-0521) nanostructures in both the samples. The intense peak at $2\theta = 28.45°$ along with other peaks at 32.90, 47.29 and 56.13° originating from (200), ($\bar{2}$02), ($\bar{1}$33) and ($\bar{3}$33) crystal planes (JCPDS 04-010-5719) can be assigned to the formation of monoclinic CTS nanostructures (major product). The presence of binary impurity in the ternary nanostructures could be due to the strong binding ability of the capping agent which causes incomplete alloying of copper sulfide and tin sulfide. Possibility of existence of secondary phases $Cu_{2-x}S$ or SnS in the desired Cu_2SnS_3 has been predicted from the chemical potential diagram of Cu-Sn-S system generated by Guan et al. [37] It has also been observed that

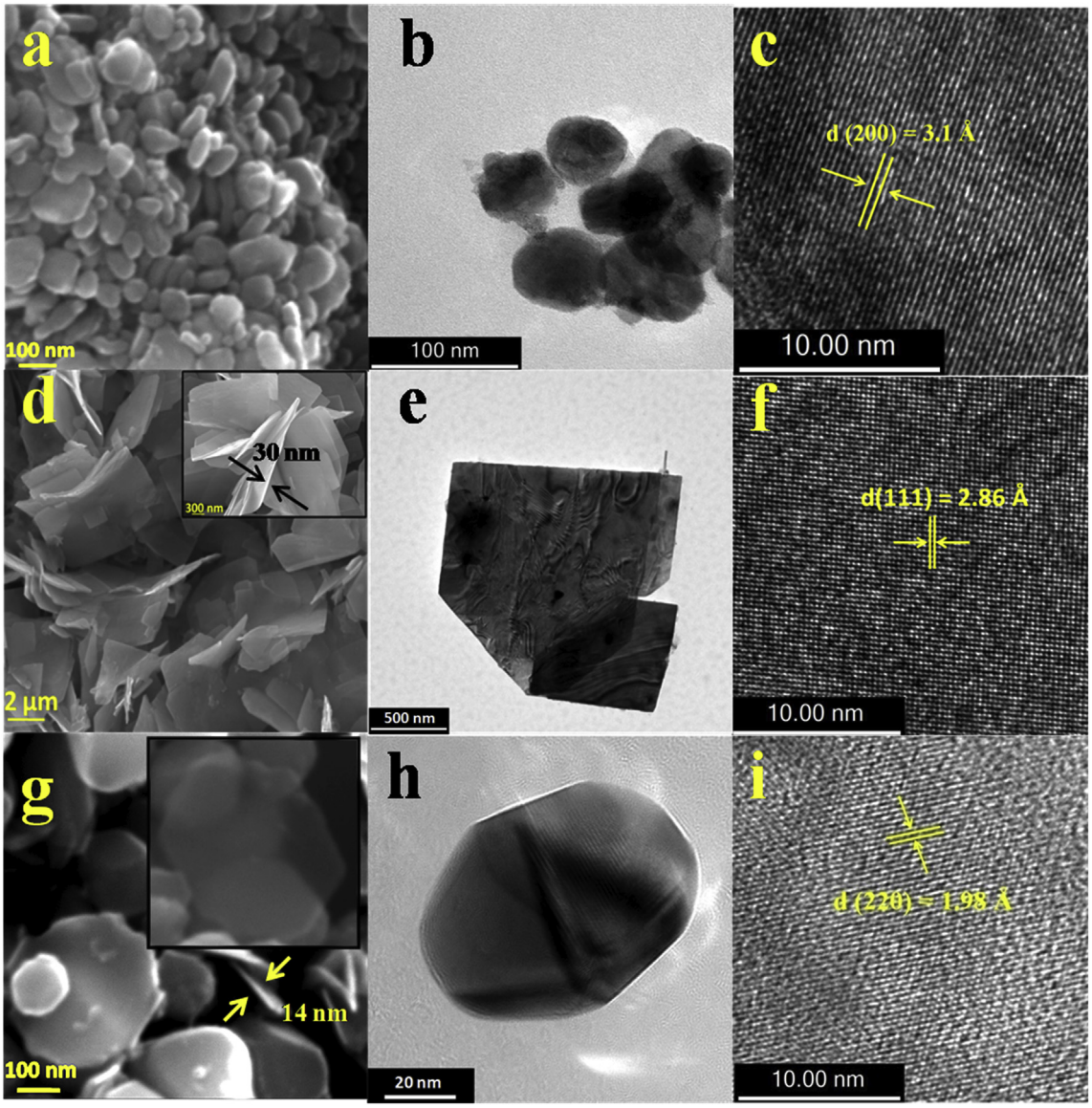

Fig. 7. SEM, TEM and HRTEM of a), b), c) monoclinic CTS obtained from thermolysis of **1** and **2;** d), e), f) orthorhombic SnS obtained from thermolysis of **1**; g), h), i) cubic $Cu_{1.8}S$ obtained from thermolysis of **2** at 300 °C for 20 min in OLA as solvent/capping agent.

formation of CuS was more prominent than SnS (Fig. 4d and e). This is possibly due to the preferential bonding of soft Lewis base (S^{2-}) with soft Lewis acid (Cu^{+}) rather than with hard Lewis acid (Sn^{4+}). Similar type of observation was recently reported by Lokhande et al. [15] The average crystallite size, calculated using Scherrer formula (Table 2) was ~15 nm for the residue obtained from OA or OA-OLA mixture. However, when relatively weak coordinating agent (OLA) was employed as a reaction solvent/capping agent, relatively larger CTS nanostructures were produced with average crystallite size ~22 nm. The corresponding PXRD (Fig. 4) showed a set of reflections (200) ($\bar{2}02$), ($\bar{1}33$) and ($\bar{3}33$) originating from the crystal planes of monoclinic CTS nanostructures (JCPDS 04-010-5719). Furthermore, the absence of peaks other than monoclinic CTS indicates that material is phase pure. The crystallinity of CTS material is reflected by sharpness of PXRD peaks. To reduce the dimensions of phase pure CTS, an effort was made by lowering down the reaction temperature to 275 °C, however the related XRD analysis shows significant contamination from orthorhombic phase of SnS in CTS nanostructures (Fig. S6) (ESI†). The lattice parameters of phase pure monoclinic CTS obtained in OLA are calculated by least square fitting and are listed in Table 3.

CTS being a ternary semiconductor material, the presence of secondary binary phases (SnS, CuS) as impurity in final product are highly probable as predicted by Guan et al. [37] In order to establish the absence of contamination from these binary phases, it is desirable to examine the formation of possible binary phases by carrying out the thermolysis of individual precursors which have been employed in the synthesis of phase pure CTS nanostructures under the similar conditions followed by the comparison of their PXRD pattern with that of CTS. Thermolysis of individual precursors in OLA at 300 °C for 20 min resulted in the formation binary SnS and $Cu_{1.8}S$ nanostructures. PXRD pattern of SnS and $Cu_{1.8}S$ are shown in Fig. S7 (ESI†). The diffraction peaks obtained in (Fig. S7c) (ESI†) are in good agreement with orthorhombic SnS (JCPDS pattern 75-0925) with preferred orientation along (013) plane. PXRD pattern shown in Fig. S7d (ESI†) can be indexed to standard JCPDS pattern 04-004-7716 of cubic phase of $Cu_{1.8}S$.

Comparative PXRD patterns of $Cu_{1.8}S$, SnS and CTS shown in Fig. 5 revealed that diffraction patterns of orthorhombic SnS and monoclinic CTS are distinctly different whereas the peak position in diffraction pattern are not markedly distinct from each other, making it difficult to distinguish CTS and $Cu_{1.8}S$ using PXRD. However, CTS and $Cu_{1.8}S$ has characteristic Raman spectra. Hence Raman spectroscopy is an important diagnostic tool to assess the phase purity of ternary CTS nanostructures.

The comparison of Raman spectra of CTS and $Cu_{1.8}S$ nanostructures obtained at 300 °C in OLA are shown in Fig. 6. The Raman spectrum of the former (Fig. 6a) is characterized by the presence of three vibrational mode peaks at 290, 315 and 349 cm^{-1} that corresponds to monoclinic phase of CTS and is in good agreement with reported literature [15,38]. The peak at 290 and 349 cm^{-1} corresponds to A′ symmetry modes while the peak at 315 cm^{-1} represents Cu-Sn atomic vibration [15,38]. The absence of characteristic vibration mode peak of $Cu_{2-x}S$ [39] at 470 cm^{-1}, (Fig. 6), rules out the possibility of contamination by binary $Cu_{2-x}S$ in ternary CTS nanostructures. The Raman data are consistent with the XRD analysis and establish the formation of phase pure monoclinic CTS devoid of binary impurities.

To further elucidate the elemental composition of the CTS nanostructures prepared in different solvent systems, energy dispersive X-ray (EDS) analysis were performed at different locations (Table 3 and Figs. S8–13) (ESI†). The studies revealed that nanostructures prepared in OA, and mixture of OA-OLA, were rich in copper and sulfur, with elemental composition $Cu_{3.4}Sn_{1.0}S_{3.8}$ (for nanostructures in OA) and $Cu_{3.6}Sn_{1.0}S_{4.4}$ (for nanostructures in a mixture of OA-OLA), while nearly stoichiometric formation of CTS nanostructures (Cu_2SnS_3) was observed when synthesized in OLA (Cu:Sn:S atom ratio is 33.4 : 15.5: 47.8 or 2.1 : 1.0:3.0). For binary nanostructures SnS and $Cu_{1.8}S$, atomic percentage was 50.1 : 49.9 (Sn:S) and 58.5 : 38.3 (Cu:S) which is fairly close to the expected value of individual grains. The elemental composition obtained from EDS analysis supports the findings discussed from XRD and Raman results. To confirm the element distribution of the as synthesized CTS, SnS and $Cu_{1.8}S$, 2-D elemental mapping of the nanostructures were recorded revealing homogeneous distribution of constituent elements within the nanocrystals (Figs. S8–13) (ESI†).

Scanning electron microscopy (SEM) and transmission electron microscopy (TEM) has been used to find the morphology and phase of the nanostructures. The SEM micrographs of nanostructures synthesized using OA showed spherical agglomeration of particles (Fig. S13) (ESI†). The SEM images shown in Figs. S15 and 16 (ESI†) represents the nanostructures synthesized in mixture of OA-OLA at 300 °C and OLA at 275 °C, respectively, which clearly showed agglomeration of particles along with the formation of rectangular sheets in former case and irregular sheets with rough edges in the case of latter. SEM, TEM and HRTEM of phase pure ternary (CTS) and binary (SnS and $Cu_{1.8}S$) nanostructures synthesized in OLA at 300 °C are shown in Fig. 7. The SEM and bright field TEM images of CTS nanostructures depicts the formation of nearly spherical particles with average diameter ~40 nm (Fig. 7a, b). The morphology of SnS and $Cu_{1.8}S$ as deduced from SEM micrographs revealed the formation of rectangular sheets and nearly hexagonal discs with smooth edges having thickness as small as ~30 nm and 14 nm, respectively (Fig. 7d, g). The TEM images of SnS and $Cu_{1.8}S$ shown in Fig. 7e and h exhibit rectangular SnS sheets and hexagonal $Cu_{1.8}S$

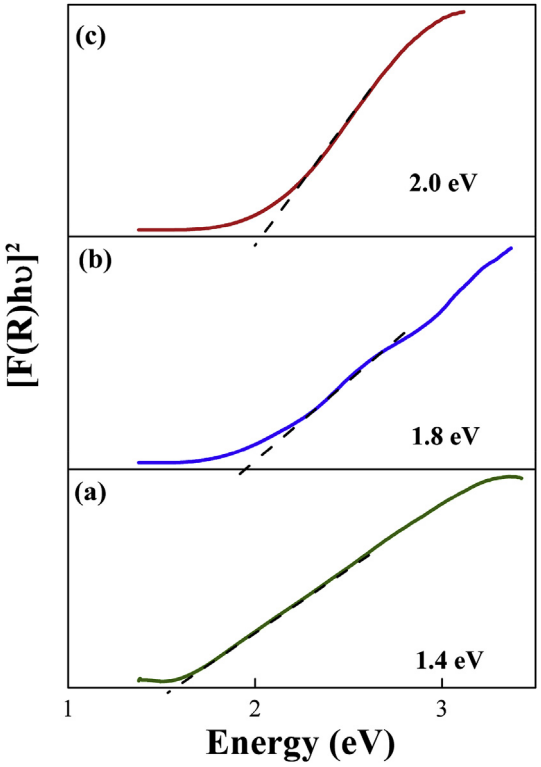

Fig. 8. Plots of [F(R)hν] [2] vs energy generated by Kubelka-Munk transformation of solid-state diffuse reflectance data of a) monoclinic CTS obtained from thermolysis of **1**and **2;** b) orthorhombic SnS obtained from thermolysis of **1**; c) cubic $Cu_{1.8}S$ obtained from thermolysis of **2** at 300 °C for 20 min in OLA as solvent/capping agent, respectively for determining direct band gap energies.

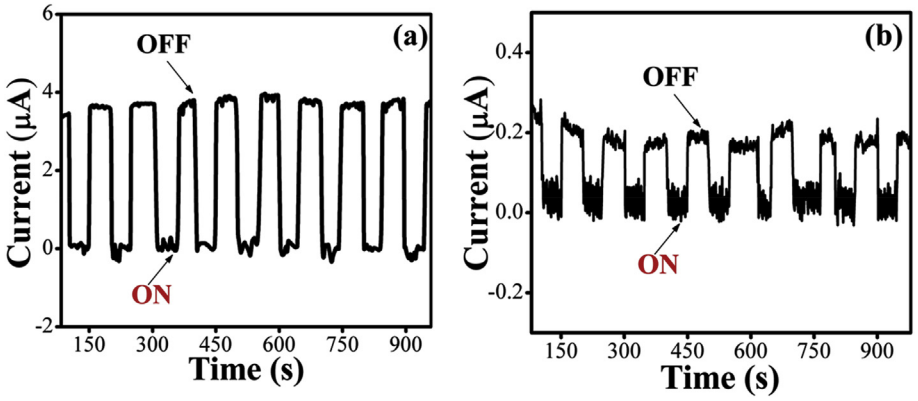

Fig. 9. Current vs Time plot phase pure a) monoclinic CTS and b) cubic $Cu_{1.8}S$, nanostructures obtained at 300 °C for 20 min using OLA as reaction solvent.

discs that are almost semi-transparent under TEM electron beam due to thin thickness. The reduced thickness of $Cu_{1.8}S$ nanostructures is also evident from the inset of Fig. 7h which shows the formation of nearly transparent hexagonal disc. The high resolution TEM (HRTEM) images of CTS, SnS and $Cu_{1.8}S$ in Fig. 7c, f, h revealed the crystalline nature of nanostructures with lattice fringe spacing 3.1, 2.86 and 1.98 Å, respectively, which can be indexed to (200) plane of monoclinic CTS (JCPDS 04-010-5719), (111) plane of orthorhombic SnS (JCPDS 75-0925) and (220) plane of cubic $Cu_{1.8}S$ (JCPDS 04-004-7716).

3.4. Optical properties

Considering the importance of CTS, SnS and $Cu_{1.8}S$ as photon absorber materials for photovoltaic cells, the optical properties of phase pure nanostructures obtained in OLA at 300 °C were investigated by diffuse reflectance spectroscopy (DRS). The optical band gaps of these materials were determined by using a plot of Kubelka-Munk function, F(R) as given in equation (1).

$$[F(R)h\nu]^{n} = A(h\nu - E_g) \quad (1)$$

where hν = photon energy, A is a constant, E_g represents the band gap and n is the exponent which depends on the nature of optical transition. The direct band gaps of CTS, SnS and $Cu_{1.8}S$ were estimated as 1.4, 1.8 and 2.0 eV, respectively by plotting the relation $[F(R)h\nu]$ [2] vs $h\nu$ derived from Tauc's model (for n = 2) (Fig. 8). These values are blue shifted with respect to bulk CTS (0.9 eV) [7], SnS (1.3 eV) [19] and $Cu_{1.8}S$ (1.2 eV) [40]. The increase in the band gap value of the nanostructures may be either due to quantum confinement or lattice distortion or surface lattice defects [24]. The direct band gap values evaluated in present investigation are consistent with those reported in literature (0.9–1.77 eV for CTS [7,15], 1.3–1.9 eV for SnS [19], and 1.2–2.3 eV for $Cu_{1.8}S$ [41]). The optimal band gap of these nanoparticles reveals their suitability as a photo-absorber material for solar cell application.

3.5. Photoelectrochemical studies

Photo-response of nanostructures (CTS, SnS and $Cu_{1.8}S$) has been evaluated by preparing photo electrochemical cell. Current-voltage (I-V) characteristics for the CTS, SnS and $Cu_{1.8}S$ nanostructures showed nonlinear behaviour (Fig. S17) (ESI†). The nonlinear I-V characteristics exhibit the junction properties with increase in current under illumination conditions relative to that of dark current due to photo-generated carriers. It has been observed that increment in photocurrent under illumination is better in case of CTS nanostructure as compared to SnS and $Cu_{1.8}S$ nanostructures. Photosensitivity and photo-stability are important criteria, to select an absorber material for photovoltaic applications. Fig. 9 shows the photo response of nanostructures (CTS, $Cu_{1.8}S$) as a function of time, measured under light intensity of 200 μW/cm^2 with bias voltages of 0.5 V. Both the material shows switching characteristics during the repeated cycles of on-off experiments. However, CTS nanostructures showed better photosensitivity and enhanced photo-response over number of on-off cycles as compared to $Cu_{1.8}S$ particles. The reproducibility of photocurrent suggests high stability of CTS nanostructures under alternating light and dark conditions. The result indicates the potential application of monoclinic CTS in photo detector and photovoltaic applications. It is worth mentioning that no such switching characteristics were observed in case of orthorhombic SnS under the same set of conditions.

4. Conclusion

The present work documents the synthesis, isolation and characterization of air stable monomeric [^{t}Bu$_2$Sn(Spyz)$_2$] (**1**) and [Cu(Spyz)(PPh$_3$)$_2$] (**2**) precursors. A convenient one pot synthesis of CTS, SnS and $Cu_{1.8}S$ nanostructures have been accomplished through thermolysis of these precursors. Phase pure CTS with nearly spherical shape, rectangular sheets of orthorhombic SnS and hexagonal morphology of cubic $Cu_{1.8}S$ were obtained in OLA while thermolysis in OA or OA-OLA leads to CTS contaminated with binary impurities. The band gap of CTS nanostructures (1.4 eV) derived from DRS, is in the range of optimum band gap required for solar energy absorption. The band gaps of nanostructures are blue shifted relative to bulk counterpart. CTS nanostructures showed better photo-response behaviour with faster switching characteristics in comparison to $Cu_{1.8}S$.

Conflicts of interest

There are no conflicts to declare.

Acknowledgement

We thank Dr. K. I. Priyadarsini, Head Chemistry Division, BARC for encouragement of this work, Dr. Bal Govind Vats (Fuel Chemistry Division) for XRD measurements and Vishal Singh (Material Science Division) for SEM measurements.

Appendix A. Supplementary data

Supplementary data to this article can be found online at https://doi.org/10.1016/j.jorganchem.2019.02.026.

References

[1] X. Liu, Y. Feng, H. Cui, F. Liu, X. Hao, G. Conibeer, D.B. Mitzi, M. Green, Prog. Photovoltaics Res. Appl. 24 (2016) 879–898.
[2] J. Ramanujam, U.P. Singh, Energy Environ. Sci. 10 (2017) 1306–1319.
[3] C. Coughlan, M. Ibanez, O. Dobrozhan, A. Singh, A. Cabot, K. Ryan, Chem. Rev. 117 (2017) 5865–6109.
[4] Y. Park, H. Jin, J. Park, S. Kim, CrystEngComm 16 (2014) 8642–8645.
[5] C. Wang, S. Chen, J. Yang, L. Lang, H. Xiang, X. Gong, A. Walsh, S. Wei, Chem. Mater. 26 (2014) 3411–3417.
[6] L. Wu, S. Chen, F. Fan, T. Zhuang, C. Dai, S. Yu, J. Am. Chem. Soc. 138 (2016) 5576–5584.
[7] Y.T. Zhai, S. Chen, J.H. Yang, H.J. Xiang, X.G. Gong, A. Walsh, J. Kang, S.H. Wei, Phys. Rev. B. 84 (2011), 075213.
[8] W. Sun, Y. Ye, Y. You, J. Xu, J. Mater. Chem. A 6 (2018) 8221–8226.
[9] M.P. Suryawanshi, U.V. Ghorpade, S.W. Shin, S.A. Pawar, I.Y. Kim, C.W. Hong, M. Wu, P.S. Patil, A.V. Moholkar, J.H. Kim, ACS Appl. Mater. Interfaces 8 (2016) 11603–11614.
[10] W. Li, X. Han, Y. Zhao, L. Liu, J. Wang, S. Yang, T. Tanaka, Mater. Lett. 125 (2014) 167–170.
[11] M. Baghbanzadeh, L. Carbone, P.D. Cozzoli, C.O. Kappe, Angew. Chem. Int. 50 (2011) 2–50.
[12] Y. Liu, M. Liu, D. Yin, W. Wei, P.N. Prasad, M.T. Swihart, Chem. Mater. 29 (2017) 3555–3562.
[13] S. Dias, K.L. Kumawat, S. Biswas, S.B. Krupanidhi, RSC Adv. 7 (2017) 23301–23308.
[14] U.V. Ghorpade, M.P. Suryawanshi, S.W. Shin, I. Kim, S.K. Ahn, J.H. Yun, C. Jeong, S.S. Kolekar, J.H. Kim, Chem. Mater. 28 (2016) 3308–3317.
[15] A.C. Lokhande, A. Shelke, P.T. Babar, J. Kim, D.J. Lee, I.C. Kim, C.D. Lokhande, J.H. Kim, RSC Adv. 7 (2017) 33737–33744.
[16] Q. Liu, Z. Zhao, Y. Lin, P. Guo, S. Li, D. Pan, X. Ji, Chem. Commun. 47 (2011) 964–966.
[17] X. Liu, X. Wang, M.T. Swihart, Chem. Mater. 27 (2015) 1342–1348.
[18] G. Kedarnath, V.K. Jain, Coord. Chem. Rev. 257 (2013) 1409–1435.
[19] A. Tyagi, G. Kedarnath, A. Wadawale, V.K. Jain, M. Kumar, B. Vishwanadh, RSC Adv. 5 (2015) 62882–62890.
[20] G.K. Kole, K.V. Vivekananda, M. Kumar, R. Ganguly, S. Dey, V.K. Jain, CrystEngComm 17 (2015) 4367–4376.
[21] R. Sharma, G. Kedarnath, V. Jain, A. Wadawale, C. Pillai, M. Nalliath, B. Vishwanadh, Dalton Trans. 40 (2011) 9194–9201.
[22] R. Sharma, A. Wadawale, G. Kedarnath, D. Manna, T. Ghanty, B. Vishwanadh, V.K. Jain, Dalton Trans. 43 (2014) 6525–6535.
[23] R. Sharma, G. Kedarnath, A. Wadawale, C. Betty, B. Vishwanadh, V.K. Jain, Dalton Trans. 41 (2012) 12129–12138.
[24] A. Tyagi, G. Kedarnath, A. Wadawale, A. Shah, V.K. Jain, B. Vishwandh, RSC Adv. 6 (2016) 8367–8376.
[25] R. Sharma, G. Kedarnath, N. Kushwah, M. Pal, A. Wadawale, B. Vishwanadh, B. Paul, V.K. Jain, J. Organomet. Chem. 747 (2013) 113–118.
[26] A. Tyagi, A.Y. Shah, G. Kedarnath, A. Wadawale, V. Singh, D. Tyagi, C.A. Betty, C. Lal, V.K. Jain, J. Mater. Sci. Mater. Electron. 29 (2018) 8937–8946.
[27] G.W.H. Cheeseman, J. Chem. Soc. (1960) 242–247.
[28] V.B. Mokal, V.K. Jain, J. Organomet. Chem. 441 (1992) 215–226.
[29] S. Dietzel, K. Jurkschat, A. Tzschach, A. Zschunke, Z. Anorg. Allg. Chem. 537 (1986) 163–168.
[30] C. Ma, J. Zhang, G. Tian, R. Zhang, J. Organomet. Chem. 690 (2005) 519–533.
[31] J. Holecek, M. Nadvornik, K. Handlir, A. Lycka, J. Organomet. Chem. 315 (1986) 299–308.
[32] M.V. Castaño, A. Macías, A. Castiñeiras, A.S. González, E.G. Martínez, J.S. Casas, J. Sordo, W. Hiller, E.E. Castellano, J. Chem. Soc. Dalton Trans. (1990) 1001–1005.
[33] R. Schmiedegen, F. Huber, H. Preut, Acta Crystallogr. C 49 (1993) 1735–1737.
[34] G. Domazetis, B.D. James, M.F. Mackay, R.J. Mayee, J. Inorg. Nucl. Chem. 41 (1979) 1555–1562.
[35] P. Karagiannidis, P. Aslanidis, D.P. Kessissoglou, B. Krebs, M. Dartmann, Inorg. Chim. Acta 156 (1989) 47–56.
[36] S.C. Davies, M.C. Durrant, D.L. Hughes, K. Leidenberger, C. Stapper, R.L. Richards, J. Chem. Soc., Dalton Trans. (1997) 2409–2418.
[37] P.W. Guan, Z.K. Liu, Phys. Chem. Chem. Phys. 20 (2018) 256–261.
[38] D.M. Berg, R. Djemour, L.G. Tay, S. Siebentritt, P.J. Dale, X. Fontane, V.I. Roca, A.P. Rodriguez, Appl. Phys. Lett. 100 (2012), 192103.
[39] T.S. Reddy, R. Amiruddin, M.C.S. Kumar, Sol. Energy Mater. Sol. Cells 143 (2015) 128–134.
[40] Y. Huang, H. Xiao, S. Chen, C. Wang, Ceram. Int. 35 (2009) 905–907.
[41] A. Sagade, R. Sharma, Sensor. Actuator. B Chem. 133 (2008) 135–143.